Science
AAAS

Supplementary Materials for

A compact synthetic pathway rewires cancer signaling to therapeutic effector release

Hokyung K. Chung[1,2,5], Xinzhi Zou[4], Veronica R. Brand[4,5], Bryce T. Bajar[4,5], Yunwen Huo[2,4,5], Javier F. Alcudia[3], James E. Ferrell Jr[6], and Michael Z. Lin[2,4,5,6]

[1]Department of Biology, Stanford University, Stanford, California, USA
[2]Department of Neurobiology, Stanford University, Stanford, California, USA
[3]Neuroscience Gene Victor & Virus Care, Stanford University, Stanford, California, USA
[4]Department of Bioengineering, Stanford University, Stanford, California, USA
[5]Department of Pediatrics, Stanford University, Stanford, California, USA
[6]Department of Chemical and Systems Biology, Stanford University, Stanford, California, USA

Correspondence to: mzlin@stanford.edu

This PDF file includes:

Materials and Methods

DNA constructs.

Plasmids encoding RASER cassettes were cloned by standard molecular biology techniques including polymerase chain reaction, restriction enzyme digestion, ligation, and homology-mediated assembly by In-Fusion enzyme (Clontech). All subcloned fragments were sequenced in their entirety to confirm successful construction. Full sequences of all plasmids used in this study are available upon request.

Chemical reagents

ErbB tyrosine kinase inhibitors lapatinib (TSZ Chem), afatinib (TSZ Chem), and osimertinib (Selleckchem) were purchased from commercial sources. HCV NS3 inhibitor asunaprevir (ASV) was obtained by custom synthesis (Acme Bioscience). For each chemical, a 1-mM stock solution in dimethylsulfoxide (Thermo Fisher) was prepared and stored at –20 ºC. Stock solutions were diluted into cell culture media to achieve final treatment concentrations of 0.5 μM for lapatinib, 1 μM for afatinib, 0.1 μM for osimertinib, or 1 μM for ASV. For cancer cell treatment in Fig. 6, 10 μM of lapatinib was used.

Antibodies

The following primary antibodies were used for immunoblotting at the indicated dilutions: mouse monoclonal anti-v5 (Thermo Scientific, R960-25), 1:2000; mouse monoclonal anti-GAPDH (Santa Cruz Biotechnology, clone G-9, sc-365062), 1:4000; rabbit polyclonal anti-GAPDH (Abcam, ab9485), 1:1000; mouse monoclonal anti-GAPDH (Pierce, clone GA1R, MA5-15738), 1:1000; rabbit monoclonal anti-phospho-EGFR/ErbB1 Tyr1173 (Cell Signaling , clone 53A5, 4407S), 1:1000; rabbit monoclonal anti-phospho-HER2/ErbB2 Tyr1221/1222 (Cell Signaling , clone 6B12, 2243S), 1:1000; rabbit monoclonal anti-cleaved PARP (Abcam, clone E51, ab32064), 1:1000; rabbit polyclonal anti-tdTomato (OriGene, TA150128), 1:2000; mouse monoclonal anti-p27 Kip1 (Cell Signaling, clone SX53G8.5, 3698T), 1:1000; rabbit monoclonal anti-Bim (Cell Signaling, clone C34C5, 2933T), 1:1000; rabbit polyclonal anti-phospho-Akt1/2/3-473 (Santa Cruz Biotechnology, sc-7985), 1:100; mouse monoclonal anti-phospho-ERK1/2 (Santa Cruz Biotechnology, clone E-4, sc-7383), 1:200. Secondary antibodies were LI-COR 680RD goat-anti-mouse, 680RD goat-anti-rabbit, 800CW goat-anti-mouse, and 800CW goat-anti-rabbit, used at 1:5000 dilution each.

Cell culture and transfection

BT-474 (ATCC), SK-BR-3(ATCC), H1975 (gift from S. Gambhir, Stanford University), Huh7.5-GFP (gift from J. Glenn, Stanford University), BxPC3 (ATCC) and 4T1 (gift from R. Levy, Stanford University) cell lines were cultured at 37 ºC in 5% CO_2 in Roswell Park Memorial Institute 1640 medium (RPMI 1640, Life Technologies) supplemented with 10% fetal bovine serum (FBS, Life Technologies), and 100 U/mL penicillin and 100 μg/mL streptomycin (Life Technologies). MCF-7 (gift from H. Chang, Stanford University), SK-OV-3 (gift from H. Dai, Stanford University), and LN-229:EGFRvIII (gift from X. Shu, UCSF) cell lines were cultured at 37 ºC in 5% CO_2 in Dulbecco's Modified Eagle's Medium (DMEM, HyClone) supplemented with 10% FBS and 100 U/mL penicillin and 100 μg/mL streptomycin. Cells were transfected using Lipofectamine 3000 (Life Technologies) in Opti-MEM (Life Technologies) according to the manufacturer's recommended protocol. The transfected populations of cells were analyzed by immunoblotting and fluorescence microscopy without replating, purification, sorting, or cloning.

Immunoblotting

After washing twice with PBS, cells were lysed with 50-100 µL of hot SDS lysis buffer (100 mM Tris HCl pH 8.0, 4% SDS, 20% glycerol, 0.2% bromophenol blue, 10% 2-mercaptoethanol), and DNA was sheared by sonication. After heating at 80-90 °C for 2-4 minutes, cell lysates were loaded onto 4%-12% Bis-Tris gels (NuPAGE, Life Technologies) along with a pre-stained Novex Sharp protein molecular weight standard (Life Technologies) or the Precision Plus protein dual-color standard (Bio-Rad). Gels were transferred to nitrocellulose membranes using a Trans-Blot Turbo Transfer System (Bio-Rad) and blocked with 10% dried nonfat milk (Carnation) in Tris-buffered saline with 0.1% Tween (PBST). Membranes were probed with primary antibodies in 10% bovine serum albumin in PBST and fluorophore-conjugated secondary antibodies in 10% dried nonfat milk in PBST, with washes in PBST after each step. Membranes were imaged using an Odyssey imaging system (LI-COR). Quantification of immunoblots was performed in ImageJ (*51*).

Generation of the molecular integrator structural model

Using UCSF Chimera (*52*), a 3D model was constructed comprising a ErbB1 cytosolic segment (PDB entry 2GS2), the SHC PTB domain interacting with pTyr-1173 (PDB entry 1SHC), NS3 (PDB entry 3M5O), the Crk SH2 domain interacting with pTyr-1016 (1JU5), mKO2 (PDB entry 2H5Q), and a modelled phospholipid bilayer interacting with the ErbB1 kinase domain (*53*). First, the C-terminal flexible region of ErbB1 was loop-modeled and docked with the SH2 and PTB domains, and energy minimization was performed. Docking sites were adapted from Hsieh et al (*54*). Finally, a published model of the complex of ErbB1 and the phospholipid bilayer (*53*) was imposed onto the 2GS2-1JU5-1SHC model.

Calculating synthesis and degradation rates of RASER components using the SMASh technique

To measure the half-lives of the SMASh-tagged RASER components, we assumed that the protein production rate is constant at the time ASV is added to induce destruction of newly synthesized protein copies (24-28 h post-transfection). The decay of previously synthesized protein copies from the time of ASV addition can be modeled with the differential equations where $P(t)$ is protein concentration of SMASh-tagged protein at time t and k_{deg} is decay rate constants of the SMASh-tagged protein:

$$dP(t)/dt = -k_{deg} \cdot P(t),$$

with $P(0)$ set to the protein amount at time zero. Integration yields:

$$P(t) = P(0)e^{-k_{deg} \cdot t}.$$

We measured half-lives ($t_{1/2}$) of the RASER components by fitting the protein band intensities of different time points to the above mono-exponential decay curve ($n = 3$). We then determined the decay rate constant (k_{deg}).

To determine k_{syn} , the protein production rate constant, the rate of changes in the protein concentrations were modeled with the following differential equation:

$$dP(t)/dt = k_{syn} - k_{deg} \cdot P(t),$$

with $P(0) = 0$. Integration yields:

$$P(t) = (k_{syn}/k_{deg}) \cdot (1 - e^{-k_{deg} \cdot t})$$

We assumed that the production rates of all RASER components are the same in the absence of lapatinib. This is because the RASER system was constructed in the bi-cistronic vector with a P2A ribosomal skipping sequence, which allows production of upstream and downstream proteins at approximately the same level (*55*). The translation rate of OFP-V5 was measured by the following process. PTBHIF-Pro::P2A::OFP-V5-SMASh was transiently transfected in the presence of ASV to block protein accumulation. After 24 h, ASV was washed out to initiate protein accumulation, and then cells were lysed for immunoblotting at various times afterwards. Amounts of detected OFP-V5 were obtained by interpolating anti-V5 band intensities to those of known amounts of purified OFP-V5. Volumes of cell lysates loaded was estimated by interpolating anti-GAPDH band intensities to those from known volumes of cell lysate, then these were multiplied by the estimated transfection efficiency to obtain the volumes of transfected cell lysates loaded. The calculated concentrations of OFP-V5 over time were fitted to the above equation with $k_{deg,\ mKO2\text{-}V5}$ previously measured as 0.026/h. k_{syn} was then calculated as 145 nM/h. All curve fits were performed in MATLAB_R2015b. The k_{syn} and k_{deg} values of each RASER components are listed in fig. S2E and fig. S4D.

Mathematical modeling of RASER

To predict the effect of ErbB hyperactivity on rates of substrate cleavage, we consider the action of ErbB as redistributing protease and, as relevant, substrate molecules to different subcellular spaces, in two RASER configurations described below.

(i) RASER system with only protease recruited to receptor: In the absence of phosphorylated ErbB (pErbB), PTB-fused protease (PTB-pro) diffuses throughout the whole cell, leading to a low background cleavage rate of membrane-tethered substrates (Supplementary Note 1). In the presence of pErbB, some molecules of PTB-pro would be recruited to the same juxtamembrane space (jm-space) as membrane-tethered substrate. Rates of cleavage of a given number of membrane-tethered substrate molecules by a given number of pErbB-bound protease molecules in one unit of time in the kinetic model (1 s) can be calculated using the Michaelis-Menten rate equation using enzyme and substrate concentrations at that time point. The presence of long linkers between the protease domain and the PTB recruitment domain, and between the substrate sequence and the farnesylation site, suggests unrestricted movement within the jm-space. We thus assume that tethering does not alter the conformation or orientation of either enzyme or substrate in a manner that affects the binding equilibrium. Thus, as in the case of membrane-tethered substrate and cytosolic protease (Supplementary Note 1), we do not assume any difference in binding free-energies for enzyme and substrate in the juxtamembrane space compared to the cytosol, and thereby use K_M values measured for the protease and substrates in solution. Note in the presence of pErbB, the fraction of PTB-pro remaining in the cytosol can still contribute to substrate cleavage at the background cleavage rate. Throughout one time point, the system is assumed to be in equilibrium maintained by multiple binding and unbinding events, so that overall distribution of receptor species (bound to PTB-pro vs. unbound) is unchanged.

Because all substrate molecules are tethered in the membrane, they can only produce product when they bind to protease molecules within the jm-space. The rate of product formation in this jm-space, $d[P]_{jm}/dt$, which has units of concentration per time, is given by

$$d[P]_{jm}/dt = d[P]_{bound}/dt + d[P]_{unbound}/dt, \qquad \text{(Eqn. 1)}$$

where $d[P]_{bound}/dt$ is the rate of product formation in the jm-space by protease bound to phospho-ErbB (pErbB) cleaving membrane-tethered substrate, and $d[P]_{unbound}/dt$ is the rate of product

formation in the jm-space by free protease diffusing throughout the cell cleaving membrane-tethered substrate.

Per the Michaelis-Menten equation,

$$d[P]_{bound}/dt = k_{cat}\cdot[pErbB{:}PTB\text{-}pro]_{jm}\cdot[S]_{jm}/([S]_{jm} + K_M),$$

where $[pErbB{:}PTB\text{-}pro]_{jm}$ is the concentration of pErbB:PTB-pro complexes in the jm-space, and $[S]_{jm}$ is the concentration of substrate in the jm-space. Also,

$$d[P]_{unbound}/dt = k_{cat}\cdot[PTB\text{-}pro]_{cell,free}\cdot[S]_{jm}/([S]_{jm} + K_M),$$

where $[PTB\text{-}pro]_{cell,free}$ is the concentration of unbound protease in the cell, which is the same as the concentration of unbound protease in jm-space due to rapid exchange as jm-space is continuous with the rest of the cell. Then,

$$\begin{aligned} d[P]_{jm}/dt &= d[P]_{bound}/dt + d[P]_{unbound}/dt \\ &= k_{cat}\cdot([pErbB{:}PTB\text{-}pro]_{jm} + [PTB\text{-}pro]_{cell,free})\cdot[S]_{jm}/([S]_{jm} + K_M) \\ &= k_{cat}\cdot[PTB\text{-}pro]_{jm,total}\cdot[S]_{jm}/([S]_{jm} + K_M), \end{aligned}$$

where $[PTB\text{-}pro]_{jm,total} = [pErbB{:}PTB\text{-}pro]_{jm} + [PTB\text{-}pro]_{jm,free}$ and represents the total effective concentration of protease in the juxtamembrane space.

$[PTB\text{-}pro]_{cell,total}$, the average concentration of total PTB-pro throughout the cell, is equivalent to $[pErbB{:}PTB\text{-}pro]_{jm}$ diluted into the whole cell plus $[PTB\text{-}pro]_{cell,free}$ or $[PTB\text{-}pro]_{jm,free}$:

$$[PTB\text{-}pro]_{cell,total} = [pErbB{:}PTB\text{-}pro]_{jm}/C_{jm} + [PTB\text{-}pro]_{cell,free}$$

where C_{jm} is a juxtamembrane space concentration conversion factor, calculated as the ratio of the volume of a cell of radius r to the volume of a juxtamembrane space of height h. As $h << r$, the volume of the juxtamembrane space can be estimated as $4\pi r^2 h$, resulting in

$$C_{jm} = (4/3\pi r^3)/4\pi r^2 h = r/3h.$$

We use a typical human epithelial cell radius of 6 μm and a jm-space height of 10 nm based on the length of the ErbB cytosolic segment, so $C_{jm} = 200$. $[PTB\text{-}pro]_{cell,free}$ can then be expressed in terms of $[pErbB{:}PTB\text{-}pro]_{jm}$ and $[PTB\text{-}pro]_{cell,total}$:

$$[PTB\text{-}pro]_{cell,free} = [PTB\text{-}pro]_{cell,total} - [pErbB{:}PTB\text{-}pro]_{jm}/C_{jm}. \qquad \text{(Eqn. 2)}$$

Thus, the effective concentration of protease in the juxtamembrane space is:

$$\begin{aligned} [PTB\text{-}pro]_{jm,total} &= [pErbB{:}PTB\text{-}pro]_{jm} + [PTB\text{-}pro]_{cell,free} \\ &= [pErbB{:}PTB\text{-}pro]_{jm}\cdot(1 - 1/C_{jm}) + [PTB\text{-}pro]_{cell,total}. \end{aligned}$$

As $C_{jm} = 200$, we can approximate $1 - 1/C_{jm}$ as simply 1, and the effective concentration of protease in the juxtamembrane space simplifies to:

$$[PTB\text{-}pro]_{jm,total} = [pErbB{:}PTB\text{-}pro]_{jm} + [PTB\text{-}pro]_{cell,total},$$

so that

$$d[P]_{jm}/dt = k_{cat}\cdot[PTB\text{-}pro]_{jm,total}\cdot[S]_{jm}/([S]_{jm} + K_M)$$
$$= k_{cat}\cdot([pErbB{:}PTB\text{-}pro]_{jm} + [PTB\text{-}pro]_{cell,total})\cdot[S]_{jm}/([S]_{jm} + K_M). \quad \text{(Eqn. 3)}$$

The quantity $[PTB\text{-}pro]_{cell,total}$ will be modelled from measured protein production and degradation rates, and $[S]_{jm}$ will be modelled from production, degradation, and cleavage rates, so the only remaining variable to calculate is $[pErbB{:}PTB\text{-}pro]_{jm}$. We can relate $[pErbB{:}PTB\text{-}pro]_{jm}$ to the known dissociation constant for pErbB:PTB-pro and the modelled $[PTB\text{-}pro]_{cell,total}$ as follows. Defining $[pErbB]_{jm,free}$ and $[pErbB]_{jm,total}$ as the concentrations of unbound and total pErbB in jm-space, respectively, then

$$[pErbB]_{jm,free} = [pErbB]_{jm,total} - [pErbB{:}PTB\text{-}pro]_{jm}, \quad \text{(Eqn. 4)}$$

where $[pErbB]_{jm,total}$ will be calculated from published measurements of total pErbB numbers per cell (*12*).

Assuming binding of pErbB and PTB is at equilibrium with a dissociation constant of $K_{D,PTB}$, then:

$$K_{D,PTB} = [pErbB]_{jm,free}\cdot[PTB\text{-}pro]_{cell,free}/[pErbB{:}PTB\text{-}pro]_{jm},$$
$$\text{or } [pErbB{:}PTB\text{-}pro]_{jm} = [pErbB]_{jm,free}\cdot[PTB\text{-}pro]_{cell,free}/K_{D,PTB}. \quad \text{(Eqn. 5)}$$

Substitution of Eqns. 2 and 4 into Eqn. 5 produces

$$[pErbB{:}PTB\text{-}pro]_{jm}$$
$$= ([pErbB]_{jm,total} - [pErbB{:}PTB\text{-}pro]_{jm})\cdot([PTB\text{-}pro]_{cell,total} - [pErbB{:}PTB\text{-}pro]_{jm}/C_{jm})/K_{D,PTB}.$$

Using x to represent $[pErbB{:}PTB\text{-}pro]_{jm}$, p to represent $[pErbB]_{jm,total}$, and q to represent $[PTB\text{-}pro]_{cell,total}$,

$$x = (p - x)\cdot(q - x/C_{jm})/K_{D,PTB},$$
$$\text{or } K_{D,PTB}\cdot x = x^2/C_{jm} - q\cdot x - p\cdot x/C_{jm} + p\cdot q,$$
$$\text{or } C_{jm}\cdot K_{D,PTB}\cdot x = x^2 - C_{jm}\cdot q\cdot x - p\cdot x + C_{jm}\, p\cdot q,$$
$$\text{or } 0 = x^2 - (p + C_{jm}\cdot q + C_{jm}\cdot K_{D,PTB})\cdot x + C_{jm}\cdot p\cdot q.$$

Per the quadratic formula,

$$x = (y \pm (y^2 - 4C_{jm}\cdot p\cdot q)^{1/2})/2, \text{ where } y = (p + C_{jm}\cdot q + C_{jm}\cdot K_{D,PTB}).$$

Restoring full names for x, p, and q,

$$[pErbB{:}PTB\text{-}pro]_{jm} = (y \pm (y^2 - 4\, C_{jm}\cdot[pErbB]_{jm,total}\cdot[PTB\text{-}pro]_{cell,total})^{1/2})/2,$$
$$\text{where } y = [pErbB]_{jm,total} + C_{jm}\cdot[PTB\text{-}pro]_{cell,total} + C_{jm}\cdot K_{D,PTB}.$$

Of the two possible solutions, only the following one converges to $[pErbB]_{jm,total}$ when $[PTB\text{-}pro]_{cell,total}$ approaches infinity and is therefore valid:

$$[pErbB{:}PTB\text{-}pro]_{jm} = (y - (y^2 - 4C_{jm}\cdot[pErbB]_{jm,total}\cdot[PTB\text{-}pro]_{cell,total})^{1/2})/2,$$
$$\text{where } y = [pErbB]_{jm,total} + C_{jm}\cdot[PTB\text{-}pro]_{cell,total} + C_{jm}\cdot K_{D,PTB}. \quad \text{(Eqn. 6)}$$

Returning to the rate of product formation in terms of concentration in the jm-space (Eqn. 3), we can now enter values for $[pErbB{\cdot}PTB\text{-}pro]_{jm}$ as calculated by Eqn. 6 and for $[PTB\text{-}pro]_{cell,total}$ as modelled from protein synthesis and degradation rates. To convert this to product formation rate in terms of concentration in the entire cell, we divide by C_{jm}, i.e.

$$d[P]_{cell}/dt = (d[P]_{jm}/dt)/C_{jm}.$$

Finally, the change over time in released cargo concentration in the cell ($[\text{released cargo}]_{cell}$) is described by

$$d[released\ cargo]_{cell} = d[P]_{cell}/dt - k_{deg,\ released\ cargo}\,[released\ cargo]_{cell},$$
$$\text{with } [released\ cargo]_{cell} = 0 \text{ M at } t = 0.$$

Changes in $[PTB\text{-}pro]_{cell,total}$ and $[S]_{cell}$ over time are described by

$$d[PTB\text{-}pro]_{cell,total}/dt = k_{syn} - k_{deg,\ PTB\text{-}pro}[PTB\text{-}pro]_{cell,total}, \text{ with } [PTB\text{-}pro]_{cell,total} = 0 \text{ M at } t = 0$$

$$\text{and } d[S]_{cell}/dt = k_{syn} - k_{deg,S}\,[S]_{cell} - d[P]_{cell}/dt, \text{ with } [S]_{cell} = 0 \text{ M at } t = 0.$$

The above ordinary differential equations were solved with MATLAB (Mathworks) using the function ode15s to obtain instantaneous values for $[released\ cargo]_{cell,}$ $[PTB\text{-}pro]_{cell,total}$, and $[S]_{cell}$ at times following introduction of RASER components into cells. Data from MATLAB were exported to Excel (Microsoft) to generate graphs.

(ii) RASER system with substrate and protease recruited to receptor: ErbB dimerizes upon overexpression or oncogenic mutation, followed by autophosphorylation (*56*), so for simplicity we assume all pErbB molecules are dimerized. If substrate can also associate directly with pErbB, then some of the PTB-pro bound at a pErbB dimer will be in the immediate vicinity of a SH2-substrate (SH2-sub) molecule bound to the dimer. For a single molecule each of PTB-pro and SH2-sub binding to a pErbB dimer, assuming confinement within a volume of radius 5 nm, the effective $[E]$ and $[S]$ each exceed 3 mM. As $[S] >> K_M$, the enzyme should be fully occupied by substrate. Product formation rate will then be the slower of k_{cat} or the time for cleaved SH2 to unbind from receptor and be replaced with another SH2-sub molecule. For HCV protease, k_{cat} is $< 0.2\ s^{-1}$, while the apparent off-rate of the high-affinity Grb2 SH2 domain to pErbB1 has been measured at $0.5\ s^{-1}$ in living cells (*57*); the off-rates of the lower-affinity SH2 domains tested for RASER are likely to be higher. Thus k_{cat} and not dissociation of cleaved SH2 is limiting for product formation, and we can estimate product formation rate as k_{cat} for each SH2-sub molecule bound to a pErbB dimer that also binds 1 or 2 molecules of PTB-pro. In addition, the remaining fraction of ErbB-bound PTB-pro will still be able to interact with the fraction of substrate molecules in the juxtamembrane space (unbound to ErbB, or bound to ErbB molecules that are not also bound to PTB-pro), at the rate described in (i) above. The fraction of PTB-pro remaining in the cytosol can also still contribute to substrate cleavage at the background cleavage rate described in (i) above. Note that throughout one unit time, the system is assumed to be in equilibrium maintained by multiple binding and unbinding events, so that overall distribution of receptor species is unchanged.

The above concepts were used to establish a model for the dually targeted RASER as follows. The rate of product formation in the jm-space, $d[P]_{jm}/dt_{dual}$, which has units of concentration per time, is given by

$$d[P]_{jm}/dt_{dual} = d[P]_{bound,bound}/dt + d[P]_{bound,unbound}/dt + d[P]_{unbound,unbound}/dt,$$

where $d[P]_{bound,bound}/dt$ is the rate of product formation by protease bound to phosphorylated ErbB (pErbB) cleaving pErbB-bound substrate, $d[P]_{bound,unbound}/dt$ is the rate of product formation by protease bound to pErbB cleaving unbound membrane-tethered substrate, and $d[P]_{unbound,unbound}/dt$ is the rate of product formation by free protease diffusing throughout the cell cleaving unbound membrane-tethered substrate, with all concentrations calculated in the jm-space. The last two terms, $d[P]_{bound,unbound}/dt$ and $d[P]_{unbound,unbound}/dt$, are identical to the terms of Eqn. 1 in part (i). Therefore, per Eqns. 3 and 6,

$$\begin{gathered} d[P]_{jm}/dt_{dual} = d[P]_{bound,bound}/dt \\ + k_{cat}\cdot([pErbB{:}PTB\text{-}pro]_{jm} + [PTB\text{-}pro]_{cell,total})\cdot[SH2\text{-}sub]_{jm,free}/([SH2\text{-}sub]_{jm,free} + K_M), \\ \text{with } [pErbB{:}PTB\text{-}pro]_{jm} = (y - (y^2 - 4C_{jm}\cdot[pErbB]_{jm,total}\cdot[PTB\text{-}pro]_{cell,total})^{1/2})/2, \\ \text{where } y = [pErbB]_{jm,total} + C_{jm}\cdot[PTB\text{-}pro]_{cell,total} + C_{jm}\cdot K_{D,PTB}. \end{gathered} \quad \text{(Eqn. 7)}$$

To calculate $d[P]_{bound,bound}/dt$, we modelled the distribution of all possible species of pErbB dimers bound to PTB-pro and/or SH2-sub. We assumed independent association of PTB and SH2, and define the fraction of pErbB bound by PTB-pro as:

$$F_{pErbB:PTB\text{-}pro/pErbB} = [pErbB{:}PTB\text{-}pro]_{jm}/[pErbB]_{jm,total}. \quad \text{(Eqn. 8)}$$

Substituting the expression for $[pErbB{:}PTB\text{-}pro]_{jm}$ from Eqn. 7 into Eqn. 8 yields

$$\begin{gathered} F_{pErbB:PTB\text{-}pro/pErbB} = (y - (y^2 - 4C_{jm}\cdot[pErbB]_{jm,total}\cdot[PTB\text{-}pro]_{cell,total})^{1/2})/2[pErbB]_{jm,total}, \\ \text{where } y = [pErbB]_{jm,total} + C_{jm}\cdot[PTB\text{-}pro]_{cell,total} + C_{jm}\cdot K_{D,PTB}. \end{gathered} \quad \text{(Eqn. 9)}$$

We define the fraction of pErbB bound by SH2-sub as:

$$F_{pErbB:SH2\text{-}sub/pErbB} = [pErbB{:}SH2\text{-}sub]_{jm}/[pErbB]_{jm,total}. \quad \text{(Eqn. 10)}$$

Unfused SH2 domains produced from earlier cleavage of SH2-sub can also associate with pErbB, but only pErbB:SH2-sub complexes contribute to product formation. Assuming cleaved SH2 and SH2-sub have the same K_D, the fraction of productive pErbB:SH2 complexes out of those involving all SH2 domains will be equivalent to the fraction of all SH2 domains consisting of uncleaved SH2-sub. For purposes of simplifying the calculation of $[pErbB{:}SH2\text{-}sub]_{jm}$, we will first calculate $[pErbB{:}anySH2]_{jm}$, the concentration of pErbB bound to any SH2 domain (cleavedSH2 or SH2-sub) in the jm-space, which can then yield $[pErbB{:}SH2\text{-}sub]_{jm}$ by proportionality:

$$\begin{gathered} [pErbB{:}SH2\text{-}sub]_{jm} = [pErbB{:}anySH2]_{jm}\cdot[SH2\text{-}sub]_{jm,total}/[anySH2]_{jm,total}, \\ \text{where } [anySH2]_{jm,total} = [SH2\text{-}sub]_{jm,total} + [cleavedSH2]_{jm,total}. \end{gathered} \quad \text{(Eqn. 11)}$$

Substituting this new definition into Eqn 10 yields

$$F_{pErbB:SH2\text{-}sub/pErbB} = ([pErbB{:}anySH2]_{jm} \cdot [SH2\text{-}sub]_{jm,total}) / ([pErbB]_{jm,total} \cdot [anySH2]_{jm,total}). \quad \text{(Eqn. 12)}$$

To calculate $[pErbB{:}anySH2]_{jm}$, we take the same approach as in (i):

$$[pErbB]_{jm,free} = [pErbB]_{jm,total} - [pErbB{:}anySH2]_{jm} \quad \text{(Eqn. 13)}$$

$$\text{and } [anySH2]_{jm,free} = [anySH2]_{jm,total} - [pErbB{:}anySH2]_{jm}, \quad \text{(Eqn. 14)}$$

where $[pErbB]_{jm,free}$ in this case refers to pErbB that is not bound to any SH2 domain.

Assuming binding of pErbB and SH2 is at equilibrium with a dissociation constant of $K_{D,SH2}$, then:

$$K_{D,SH2} = [pErbB]_{jm,free} \cdot [anySH2]_{jm,free} / [pErbB{:}anySH2]_{jm},$$
$$\text{or } K_{D,SH2} \cdot [pErbB{:}anySH2]_{jm} = [pErbB]_{jm,free} \cdot [anySH2]_{jm,free}. \quad \text{(Eqn. 15)}$$

Substitution of Eqns. 13 and 14 into Eqn. 15 produces:

$$K_{D,SH2} \cdot [pErbB{:}anySH2]_{jm} = ([pErbB]_{jm,total} - [pErbB{:}anySH2]_{jm}) \cdot ([anySH2]_{jm,total} - [pErbB{:}anySH2]_{jm}).$$

Using x to represent $[pErbB{:}anySH2]_{jm}$, p to represent $[pErbB]_{jm,total}$, and q to represent $[anySH2]_{jm,total}$,

$$K_{D,SH2} \cdot x = (p - x) \cdot (q - x),$$
$$\text{or } K_{D,SH2} \cdot x = x^2 - q \cdot x - p \cdot x + p \cdot q,$$
$$\text{or } 0 = x^2 - (p + q + K_{D,PTB}) \cdot x + p \cdot q.$$

Per the quadratic formula,

$$x = (z \pm (z^2 - 4pq)^{1/2})/2, \text{ where } z = (p + q + K_{D,SH2}).$$

Restoring full names for x, p, and q,

$$[pErbB{:}anySH2]_{jm} = (z \pm (z^2 - 4[pErbB]_{jm,total} \cdot [anySH2]_{jm,total})^{1/2})/2,$$
$$\text{where } z = [pErbB]_{jm,total} + [anySH2]_{jm,total} + K_{D,SH2}.$$

Of the two solutions, only one converges to $[pErbB]_{jm,total}$ when $[anySH2]_{jm,total}$ approaches infinity and is therefore valid:

$$[pErbB{:}anySH2]_{jm} = (z - (z^2 - 4[pErbB]_{jm,total} \cdot [anySH2]_{jm,total})^{1/2})/2,$$
$$\text{where } z = [pErbB]_{jm,total} + [anySH2]_{jm,total} + K_{D,SH2}. \quad \text{(Eqn. 16)}$$

Note per Eqn. 11,

$$[pErbB{:}SH2\text{-}sub]_{jm} = [pErbB{:}anySH2]_{jm} \cdot [SH2\text{-}sub]_{jm,total} / [anySH2]_{jm,total}$$
$$= (z - (z^2 - 4[pErbB]_{jm,total} \cdot [anySH2]_{jm,total})^{1/2} \cdot [SH2\text{-}sub]_{jm,total}) / 2[anySH2]_{jm,total},$$
$$\text{where } z = [pErbB]_{jm,total} + [anySH2]_{jm,total} + K_{D,SH2}. \quad \text{(Eqn. 17)}$$

Substituting Eqn. 16 into Eqn. 12, or Eqn. 17 into Eqn. 10, yields:

$$F_{pErbB:SH2\text{-}sub/pErbB} = (z - (z^2 - 4[pErbB]_{jm,total}\cdot[anySH2]_{jm,total})^{1/2})\cdot[SH2\text{-}sub]_{jm,total}/(2[anySH2]_{jm,total}\cdot[pErbB]_{jm,total}),$$
$$\text{where } z = [pErbB]_{jm,total} + [anySH2]_{jm,total} + K_{D,SH2}. \quad \text{(Eqn. 18)}$$

To calculate the number of cleavage events in j-space in the ErbB-on state, we considered four states of an individual pErbB chain. The fractions of each state are:

$$F_{pE:p,s} := \text{Fraction of pErbB chains bound to both PTB-pro and SH2-sub} = F_{pErbB:PTB\text{-}pro/pErbB}\cdot F_{pErbB:SH2\text{-}sub/pErbB},$$

$$F_{pE:p,0} := \text{Fraction of pErbB chains bound to PTB-pro only} = F_{pErbB:PTB\text{-}pro/pErbB}\cdot(1 - F_{pErbB,SH2\text{-}sub/pErbB}),$$

$$F_{pE:0,s} := \text{Fraction of pErbB chains bound to SH2-sub only} = F_{pErbB,SH2\text{-}sub/pErbB}\cdot(1 - F_{pErbB,PTB\text{-}pro/pErbB}),$$

$$F_{pE:0,0} := \text{Fraction of pErbB chains bound to neither} = (1 - F_{pErbB,PTB\text{-}pro/pErbB})\cdot(1 - F_{pErbB,SH2\text{-}sub/pErbB}).$$

Four states of pErbB dimers contain at least one molecule each of bound PTB-pro or SH2-sub, thereby mediating product formation at a rate limited by SH2 exchange. These four states occur at the following frequencies:

$$F_{2pE:1p,1s} := \text{Fraction of pErbB dimers bound to 1 PTB-pro and 1 SH2-sub} = F_{pE:p,s}\cdot F_{pE:0,0} + F_{pE:p,0}\cdot F_{pE:0,s},$$

$$F_{2pE:1p,2s} := \text{Fraction of pErbB dimers bound to 1 PTB-pro and 2 SH2-sub} = F_{pE:p,s}\cdot F_{pE:0,s},$$

$$F_{2pE:2p,1s} := \text{Fraction of pErbB dimers bound to 2 PTB-pro and 1 SH2-sub} = F_{pE:p,s}\cdot F_{pE:p,0},$$

$$F_{2pE:2p,2s} := \text{Fraction of pErbB dimers bound to 2 PTB-pro and 2 SH2-sub} = F_{pE:p,s}\cdot F_{pE:p,s}.$$

When pErbB dimers bind PTB-pro and SH2-sub simultaneously, we can assume full enzyme occupancy. The rate of product formation per pErbB dimer will be limited by the number of PTB-pro or SH2-sub molecules, whichever is fewer. Among pErbB dimers binding both PTB-pro and SH2-sub, product formation rate will be k_{cat} if either one PTB-pro or one SH2-sub molecule is bound, and $2k_{cat}$ if two PTB-pro and two SH2-sub molecules are bound.

Because the concentration of dimers in the jm-space is $[pErbB]_{jm,total}/2$, the total product formation rate from cleavage of pErbB-bound SH2-sub molecules is given by:

$$d[P]_{bound,bound}/dt = k_{cat}\cdot[pErbB]_{jm,total}\cdot(F_{2pE:1p,1s} + F_{2pE:1p,2s} + F_{2pE:2p,1s} + 2F_{2pE:2p,2s})/2. \quad \text{(Eqn. 19)}$$

Substituting Eqns. 16 into Eqn. 7, the total rate of cleavage is given by

$$d[P]_{jm}/dt_{dual} = k_{cat}\cdot[pErbB]_{jm,total}\cdot(F_{2pE:1p,1s} + F_{2pE:1p,2s} + F_{2pE:2p,1s} + 2F_{2pE:2p,2s})/2 + \frac{k_{cat}\cdot([pErbB:PTB\text{-}pro]_{jm} + [PTB\text{-}pro]_{cell,total})\cdot[SH2\text{-}sub]_{jm,free}}{([SH2\text{-}sub]_{jm,free} + K_M)}. \quad \text{(Eqn. 20)}$$

Substituting $[SH2\text{-}sub]_{jm,free} = [SH2\text{-}sub]_{jm,total} - [pErbB:SH2\text{-}sub]_{jm}$ yields:

$$d[P]_{jm}/dt_{dual} = k_{cat}\cdot[pErbB]_{jm,total}\cdot(F_{2pE:1p,1s} + F_{2pE:1p,2s} + F_{2pE:2p,1s} + 2F_{2pE:2p,2s})/2 + \frac{k_{cat}\cdot([pErbB:PTB\text{-}pro]_{jm} + [PTB\text{-}pro]_{cell,total})\cdot([SH2\text{-}sub]_{jm,total} - [pErbB:SH2\text{-}sub]_{jm})}{([SH2\text{-}sub]_{jm,total} - [pErbB:SH2\text{-}sub]_{jm} + K_M)}, \quad \text{(Eqn. 21)}$$

where the two concentrations $[pErbB:PTB\text{-}pro]_{jm}$ and $[pErbB:SH2\text{-}sub]_{jm}$ are as described by Eqns. 6 and 17:

$$[pErbB:PTB\text{-}pro]_{jm} = (y - (y^2 - 4C_{jm}\cdot[pErbB]_{jm,total}\cdot[PTB\text{-}pro]_{cell,total})^{1/2})/2,$$
where $y = [pErbB]_{jm,total} + C_{jm}\cdot[PTB\text{-}pro]_{cell,total} + C_{jm}\cdot K_{D,PTB}$, and

$$[pErbB:SH2\text{-}sub]_{jm} = (z - (z^2 - 4[pErbB]_{jm,total}\cdot[anySH2]_{jm,total})^{1/2}\cdot[SH2\text{-}sub]_{jm,total})/2[anySH2]_{jm,total},$$
where $z = [pErbB]_{jm,total} + [anySH2]_{jm,total} + K_{D,SH2}$
and $[anySH2]_{jm,total} = [SH2\text{-}sub]_{jm,total} + [cleavedSH2]_{jm,total}$.

To convert this to product formation rate in whole-cell concentration terms, we divide by C_{jm}, i.e.

$$d[P]_{cell}/dt_{dual} = (d[P]_{jm}/dt_{dual})/C_{jm}.$$

Finally, the change over time in released cargo concentration in the cell ($[released\ cargo]_{cell}$) is described by:

$$d[released\ cargo]_{cell} = d[P]_{cell}/dt_{dual} - k_{deg,\ released\ cargo}\,[released\ cargo]_{cell},$$
with $[released\ cargo]_{cell} = 0$ at $t = 0$.

Changes in $[PTB\text{-}pro]_{cell,total}$, $[SH2\text{-}sub]_{cell,total}$, and $[cleavedSH2]_{cell,total}$ over time are given by:

$$d[PTB\text{-}pro]_{cell,total}/dt = k_{syn} - k_{deg,\ PTB\text{-}pro}[PTB\text{-}pro]_{cell,total},$$
with $[PTB\text{-}pro]_{cell,total} = 0$ at $t = 0$,

$$d[SH2\text{-}sub]_{cell,total}/dt = k_{syn} - k_{deg,SH2\text{-}sub}\,[SH2\text{-}sub]_{cell,total} - d[P]_{cell}/dt_{dual},$$
with $[SH2\text{-}sub]_{cell,total} = 0$ at $t = 0$,

and $d[cleavedSH2]_{cell,total}/dt = d[P]_{cell}/dt_{dual} - k_{deg,cleavedSH2}\,[cleavedSH2]_{cell,total},$
with $[cleavedSH2]_{cell,total} = 0$ at $t = 0$.

$[SH2\text{-}sub]_{jm,total}$ was then calculated as $C_{jm}\cdot[SH2\text{-}sub]_{cell,total}$, and $[cleavedSH2]_{jm,total}$ as $C_{jm}\cdot[cleavedSH2]_{cell,total}$.

The above ordinary differential equations were solved with MATLAB using the function ode15s to obtain values for $[released\ cargo]_{cell}$, $[PTB\text{-}pro]_{cell,total}$, and $[S]_{cell}$ at times following introduction of RASER components into cells. Data from MATLAB were exported to Excel to generate graphs.

Imaging of cargo release and transcriptional reporter expression

Cells were cultured in 12-well plastic-bottom plates or 96-well glass-bottom plates (Greiner) and imaged in culture media using an Axiovert 200M inverted epifluorescence microscope (Zeiss) with a 10× 0.5-NA or a 20× 0.57-NA air objective and a Texas Red filter set connected to an ORCA-ER camera (Hamamatsu) and controlled by Micro-Manager software as previously described[35]. Image intensities were scaled to the same range for each channel within an experiment using ImageJ.

Virus preparation and infection

To package lentivirus, HEK293T cells at ~70% confluency were transfected with psPAX2, pMD2.G, and pLL3.7 plasmids using Lipofectamine 2000 (Life Technologies). Two days following transfection, viral supernatant was filtered with a 0.45 μm PES filter before using to infect target cells. rAAVdj-CAG-RASER1C-mCardinal-Bid and rAAVdj-mCardinal were produced at the Stanford Gene Vector and Virus Core (Stanford University). Virus infected cells were neither sorted nor purified prior to obtaining the results shown, to remain close to the actual use scenario.

Caspase-3 activity assay

NucView 488 Caspase-3 substrate (Biotium) and Hoechst 33342 (Invitrogen) were diluted into culture media to final concentrations of 1 μM each. After 1 h of incubation, cells were imaged with the Axiovert 200M with a 10× 0.5-NA air objective.

Cell viability assay

The cytotoxicity of 5 μM staurosporine (Apex Bio, as a positive control for apoptosis), 10 μM carboplatin (Santa Cruz Biotechnology) + 10 μM paclitaxel (Apex Bio), 10 μM lapatinib (TSZ Chem), ErbB-RASER1C-Bid-OFP lentivirus (MOI 2), or control mKO2 lentivirus (MOI 2) were tested in BT-474, H1975, MCF-7, MCF-10A and MRC-5 cells. For each condition, relative viability was assessed using the fluorogenic live cell marker Gly-Phe-AFC (CellTiter-Fluor Cell Viability Assay kit, Promega) and an Infinite M1000 spectrofluorimeter (TECAN) according to the manufacturer's protocol. A cytotoxicity index was calculated by subtracting the Gly-Phe-AFC signal of each condition from that of the mKO2-only lentivirus condition, followed by normalization to the value for staurosporine.

RASER testing in a model of disseminated cancer

GFP-expressing Huh7.5 cells were cultured in 1% DMSO + 10% FBS + RPMI to differentiate into a non-proliferating mature hepatocyte phenotype that can be maintained for weeks in monolayer. At day 4 of differentiation, 20,000 of ErbB+ pancreatic cancer cell line (BxPC3) or ErbB– breast tumor cell line (MCF-7) were co-cultured. Both cancer cell lines were marked with CellTracker™ Orange CMTMR (Invitrogen). After 24 h of co-culture, either rAAV-RASER1C-Bid or control rAAV were treated for a designated time with specified MOI. Viable cells were counted and expressed as a fraction of the number of cells in the negative control of the first experiment (MOI 0 condition for Fig. S14 and control rAAV infection for Fig. 6). The cytotoxic fraction was then calculated as 1 minus the viable fraction.

Guide RNA sequences

The spacer (variable) sequences of guide RNAs tested for activation of the *CSF2* (GM-CSF) promoter were:

gRNA 1: GTGACCACAAAATGCCAGGG,
gRNA 2: CGGGGGAACTACCTGAACTG,
gRNA 3: GGCCCTTATCAGCCACACAT,
gRNA 4: CGGTGAGCCTTTTCCCTAGG,
gRNA 5: TTATCAGCCACACATGGGAA,
gRNA 6: GCCAGGAGATTCCACAGTTC,
gRNA 7: TGGGCTGTCGGTTCTTGGAA,
gRNA 8: CCACCCACCCGCCTTCCTGA,
gRNA 9: TGGAGAGCCCTCAGGAAGGC,
gRNA 10: GGCTGCCCCCTCCCTCTGAG.

gRNAs 1-3 were from ref. (*58*). gRNAs 4-6 were from ref. (*27*). gRNAs 7-10 were from ref. (*59*).

Statistical analyses

Statistical analyses were performed using the Prism7 program (GraphPad). Given preliminary measurements of effect size and variability, we determined a sample size of 3 biological replicates would provide sufficient power to achieve an alpha level of 0.05. To test for significant differences between ErbB states or cell types for a given RASER variant, data distributions were first assessed for normality using the Anderson-Darling test. In all cases, data distributions fit a normal distribution except for the mCherry brightness measurements of Fig. 5C and fig. S12C. To assess the significance of differences in RASER output between EGF stimulation conditions in MCF-7 cells (Fig. 3B), one-way analysis of variance (ANOVA). To assess the significance of increased RASER output in an ErbB-on condition above the baseline (ErbB-off) condition in the same cell type (Fig. 3B, Fig. 5C, and fig. S12C), one-tailed unpaired t tests were performed. To detect any differences in endogenous Akt and Erk activation in RASER-expressing and RASER-nonexpressing conditions in the same cell type (Fig. 3C), two-tailed unpaired t tests were performed. To assess the significance of increased RASER output in ErbB-hyperactive cancer cells over an ErbB-normal control cell (Fig. 4C, Fig. 4F, Fig. 5F, fig. S10, and fig. S11), one-tailed unpaired t tests were performed, with Bonferroni correction of p-values for multiple comparisons where appropriate (Fig. 4F). For Fig.4, Fig. 6, and fig. S14, single-factor ANOVA followed by Holm-Sidak's multiple comparisons test was performed. To assess the significance of differences in mCherry expression in combinations of ErbB activity and RASER or dCas9VP64 expression (Fig. 5C and fig. S12C), differences between multiple conditions were assessed using the non-parametric Kruskal-Wallis test followed by a Dunn’s posthoc test for pairwise comparisons.

Supplementary Text

Calculating the effect of membrane tethering of substrate in suppressing cleavage by protease

To determine the effectiveness of membrane tethering of substrate in suppressing basal cleavage by a cytosolic protease, we calculated cleavage rates when substrate is either cytosolic or membrane-bound. If both protease and substrate are diffusely cytosolic, cleavage rate according to the Briggs and Haldane formulation of the Michaelis-Menten equation is

$$dP_{free,free}/dt = k_{cat}\cdot[E]\cdot[S]/([S] + K_M),$$

where $dP/dt_{free,free}$ is the product formation rate assuming free cytosolic localization of substrate and protease, [E] is mean enzyme concentration throughout the cytosol, [S] is mean substrate concentration throughout the cytosol, and K_M is the Michaelis constant measured under standard-conditions, equal to $(k_{off} + k_{cat})/k_{on}$.

If enzyme remains free in the cytosol while the same total amount of substrate becomes membrane-bound, cleavage occurs only by protease in a juxtamembrane space (jm-space), which can be estimated as

$$dP_{free,memb}/dt = k_{cat}\cdot[E]\cdot[S]_{jm}/([S]_{jm} + K_M)$$
$$\text{where } [S]_{jm} = C_{jm}\cdot[S].$$

Here, C_{jm} is a juxtamembrane space concentration conversion factor, calculated as the ratio of the volume of a cell of radius r to the volume of a jm-space volume of height h, estimated as

$$C_{jm} = (4/3\pi r^3)/4\pi r^2 h = r/3h.$$

We estimate a cell radius of 6 μm and a jm-space height of 10 nm, so $C_{jm} = 200$.

We considered whether enzyme-substrate pairs would exhibit a different apparent K_M when the substrate is membrane-tethered compared to the value measured with freely diffusing substrate. For instance, almost all enzyme-substrate collisions will involve enzyme diffusing from the cytosolic side of the substrate, so the 2-fold reduction in possible approach angles can be expected to lead to a 2-fold reduction in the frequency of collisions between enzyme and substrate and a corresponding decrease in k_{on}. As $K_M = (k_{off} + k_{cat})/k_{on}$, this might be expected to increase K_M. However, the same membrane that prevents approach from one side will also reduce k_{off}, by either sterically preventing dissociation from one side, or restricting diffusion immediately after dissociation and allowing re-association. These individual changes are impossible to predict with certainty a priori, but whether overall K_M is likely to change can be considered in energetic terms. For sequence-specific viral proteases HCV NS3 and TEV, $k_{off} >> k_{cat}$ (for HCV NS3 protease with NS4a cofactor and an optimal substrate, $k_{cat} = 0.6\ s^{-1}$ while $k_{off} = 86\ s^{-1}$, where k_{off} was calculated from the equation $k_{off} = k_{on}\cdot K_M - k_{cat}$ using measured values for k_{on}, K_M, and k_{cat} of 2.7 $\mu M^{-1}\ s^{-1}$, 32 μM, and 0.6 s^{-1}, respectively (*16*, *60*). K_M is therefore essentially equivalent to K_D. The K_D of an interaction is $e^{-\Delta G/RT}$ where ΔG is the free energy change upon enzyme-substrate binding. Given that the substrate is tethered via a flexible linker, there is no reason to expect a change in the ΔG of enzyme-substrate binding. For example, there is no reason to expect that the substrate sequence assumes a different conformation after tethering in a way that affects enzyme binding, or that it is located close enough to the membrane to hinder enzyme access. Thus we assume energetics are not changed by membrane tethering, which would suggest that K_D (and thereby K_M) are also not changed. Assumptions of unaltered energetics when tethers are added or removed is standard in

the field, and are why the K_D between a phosphorylated transmembrane receptor and cytosolic SH2- or PTB-containing proteins in a cell is assumed to be well represented by the K_D between a soluble phosphopeptide and a surface-bound SH2 or PTB domain (*61*).

In the case where enzyme is cytosolic while substrate is membrane-bound, cleavage only occurs in $1/C$ of the cell volume, so the relative total cleavage in a cell with membrane vs cytosolic localization of substrate, for the same total number of substrate molecules per cell, is

$$(1/C_{jm})(dP_{free,memb}/dt)/(dP_{free,free}/dt) = ([S] + K_M)/([S]_{jm} + K_M) = ([S] + K_M)/(C_{jm}\cdot[S] + K_M).$$

This equation shows that total cleavage with membrane-bound substrate will be lower than with the same amount of cytosolic substrate across all possible substrate numbers, confirming membrane tethering suppresses substrate cleavage by cytosolic protease. The suppressing effect becomes negligible as $[S]$ approaches zero, and approaches $1/C_{jm}$ for $[S] >> K_M$.

We plotted $dP/dt_{cyto,cyto}$ and $dP/dt_{jm,memb}$ using k_{cat} and K_M values for the site-specific tobacco etch virus (TEV) protease and hepatitis C virus (HCV) NS3 protease (with or without the NS4A cofactor). The results confirmed that membrane sequestration should reduce basal cleavage by a cytosolic protease, especially as substrate amounts increase (fig. S1C).

Calculating protein degradation and production rates

To calculate protein degradation and production rates, we used the SMASh tag (*18*). This polypeptide tag contains a degron that is removed by cis-proteolysis by a linked NS3 protease. In the absence of a drug, NS3 protease activity causes the SMASh tag to be removed from proteins as they are produced, so the proteins are not degraded. Addition of a NS3 protease inhibitor, such as asunaprevir (ASV), blocks tag removal on subsequently synthesized proteins, causing effective shutoff of further protein production. The degradation of protein copies produced before drug application can then be followed over time immunoblotting (fig. S2B to D). The decay rates of all components were experimentally determined using this method (fig. S2E).

Translation kinetics were measured using a reverse SMASh technique, in which protein accumulation is first suppressed by ASV. ASV is then washed out and immunoblotting performed at various times afterwards. Measurements of band intensities relative to concentration standards allows quantitation of the amount of protein synthesized over time (fig. S2F to G).

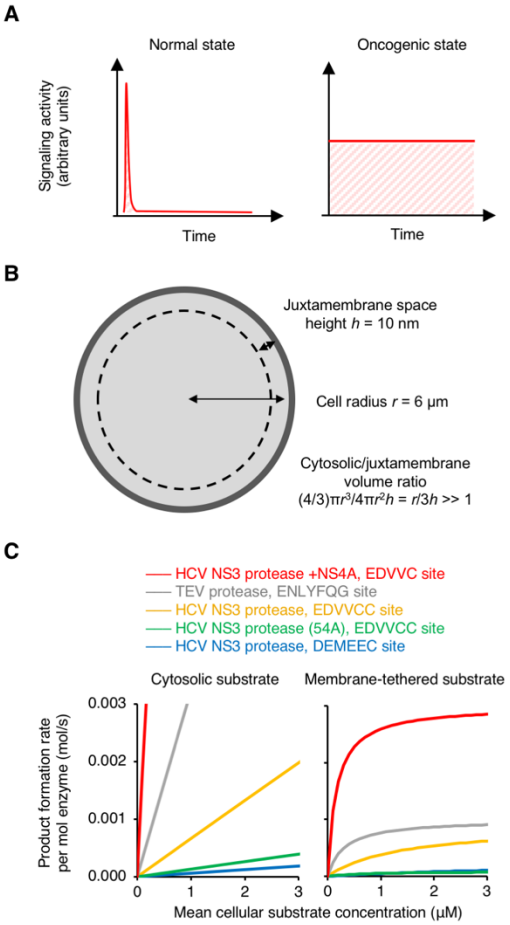

D

Model parameter	Value or source
ShcPTB-phosphoErbB dissociation constant	47 nM (*11*)
ShcPTB-protease synthesis rate	fig. S2H
ShcPTB-protease degradation rate	fig. S2E, S5D
cargo-substrate-CAAX synthesis rate	fig. S2H, S4E
cargo-substrate-CAAX degradation rate	fig. S2E, S4D
cargo degradation rate	fig. S2E
substrate-CAAX degradation rate	fig. S2E
protease-substrate Michaelis constant	fig. S1E
protease catalytic turnover rate	fig. S1E
phosphoErbB molecules/cell	fig. S1F
juxtamembrane volume	fig. S1B, Fig. 1C

E

Substrate	Protease	k_{cat} (s^{-1})	K_M (μM)	Ref.
EDVVCC	NS3(54A)	0.018	135	(*16, 17*)
DEMEEC	NS3(54A)	0.005	403	(*16, 17*)
EDVVCC	NS3	0.18	270	(*16*)
DEMEEC	NS3	0.05	805	(*16*)

F

Cell line	Origin	ErbB activation mechanism	pErbB1 # per cell	pErbB2 # per cell	mAb/TKI-sensitive	Ref.
MCF-7	breast	none	NA	NA	no	(*13*)
BT-474	breast	overexpression	4330	2360	yes	(*12, 13*)
SK-BR-3	breast	overexpression	7520	2760	yes	(*12, 13*)
SK-OV-3	ovary	overexpression	38700	2860	yes	(*12, 13*)
NCI-H1975	lung	overexpression, point mutation	130000	ND	yes	(*12, 14,15*)
LN-229:EGFRvIII	brain	overexpression, deletion mutation	ND	ND	yes	(*20*)

Fig. S1. Modeling confirms the benefit of protease-substrate segregation and model parameters (**A**) Integrated signal is higher in oncogenic than in normal signaling. (**B**) Cells are assumed to be spheres with radius (*r*) of 10 μm. The juxtamembrane space where membrane tethered substrates are located has a height (*h*) of 10 nm, based on an atomic model (Fig. 1C). (**C**) Calculation of cleavage rates of cytosolic substrate and membrane-localized substrate by cytosolic protease in (B). (**D**) Model parameters and their values. (**E**) Enzymatic parameters of HCV NS3 protease and substrate pairs. To estimate k_{cat} and K_M of NS3(54A) with EDVVCC or DEMEEC substrates, the k_{cat} and K_M values measured for the wild-type NS3 protease domain with these substrates (ref. 16) were adjusted by the fold decrease in k_{cat} and increase in K_M caused by the 54A mutation in the HCV protease holoenzyme, consisting of NS3 protease domain and the NS4A β-strand cofactor (ref. 17). (**F**) Numbers of phospho-ErbB proteins per cell. For SK-BR-3 and SK-OV-3, the ratio of phospho-ErbB:total ErbB observed in BT-474 cells and the total number of cell surface ErbB molecules was used to estimate numbers of phospho-ErbB molecules.

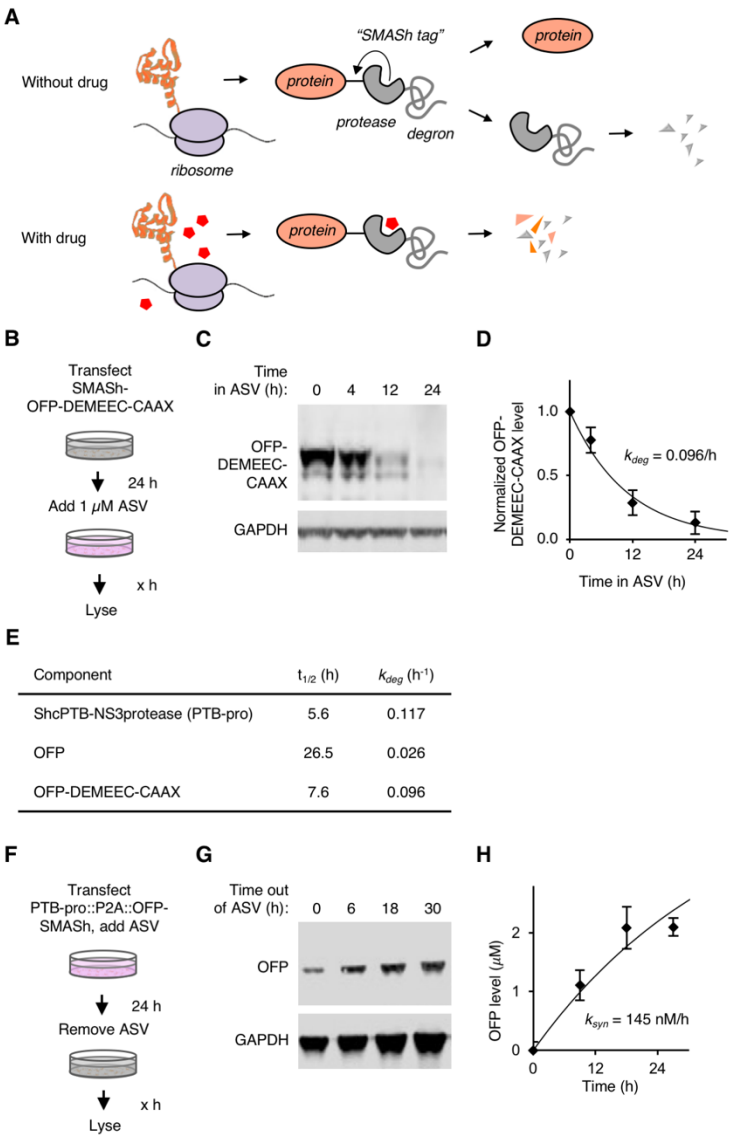

Fig. S2. Modeling parameters are determined using the SMASh technique. (**A**) Schematic description of the SMASh system. A self-removing degron permits protein production until a HCV NS3 protease inhibitor is added. (**B**) Experimental scheme for measuring protein half-life, using OFP-DEMEEC-CAAX as an example. 24 h after transfection with SMASh-tagged OFP-DEMEEC-CAAX, further synthesis is abolished at time 0 by adding the HCV NS3 protease inhibitor asunaprevir (ASV), and protein levels are measured over time. (**C**) Example immunoblot measuring OFP-DEMEEC-CAAX levels over time. (**D**) Quantitation of OFP-DEMEEC-CAAX levels over time (n = 3, error bar = s.e.m). OFP-DEMEEC-CAAX levels were normalized to GAPDH and fit to an exponential decay curve. (**E**) Degradation rates of prototypical RASER components. (**F**) Experimental procedure for obtaining protein synthesis rate with PTB-pro::P2A::OFP-SMASh. The construct expressing cells were incubated in ASV for 24 h, synthesis of the protein was permitted by removal of ASV, and the protein levels were measured over time. (**G**) Quantitation of OFP levels over time (n = 3, error bar = s.e.m). OFP levels were normalized to GAPDH and fit to a function assuming a constant synthesis rate and a previously measured degradation rate. The determined synthesis rate of OFP was used to represent that of the protease component upstream to the P2A sequence, as the protease, the P2A peptide, and the downstream open reading frame encoding the substrate are all translated as a single polypeptide.

A

binding domain	K_D with ErbB1/EGFR	pTyr binding site (aa)	K_D with ErbB2/HER2	pTyr binding site (aa)
PIK3R1 SH2 (NT)	646 nM	1016	508 nM	1139
PIK3R2 SH2 (NT)	425 nM	1016	281 nM	
PIK3R3 SH2 (CT)	193 nM	1016	304 nM	
SYK SH2 (CT)	934 nM	1016	240 nM	
VAV1 SH2	1 μM	1016	206 nM	
PLCG1 SH2 (CT)	2 μM	1016	1.9 μM	
CRK SH2	407 nM	1016	848 nM	1196

B

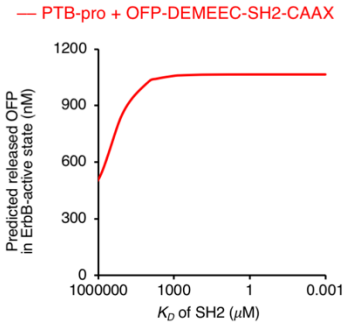

Fig. S3. Modeling of the dual-targeting system. (**A**) Dissociation constants and binding site specificities of candidate SH2 domains. (**B**) To find out the optimal affinity of SH2 to the active receptor, different K_D values of SH2 were tested with the model.

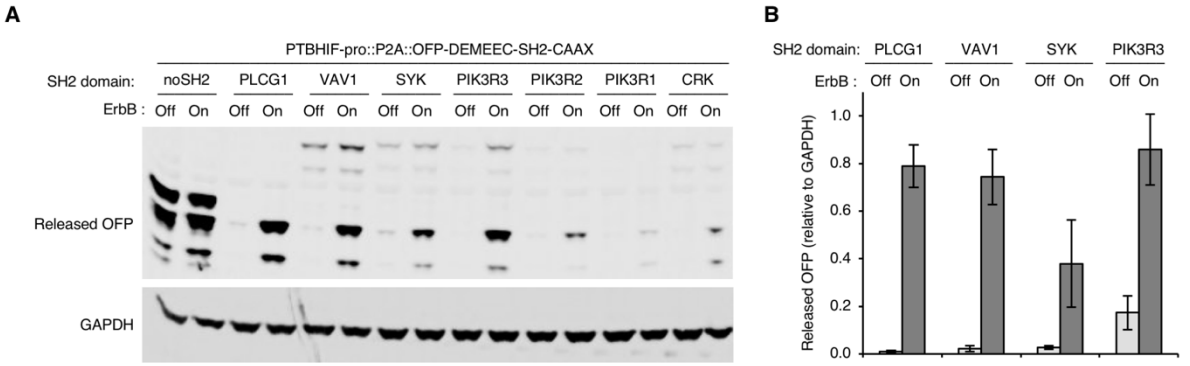

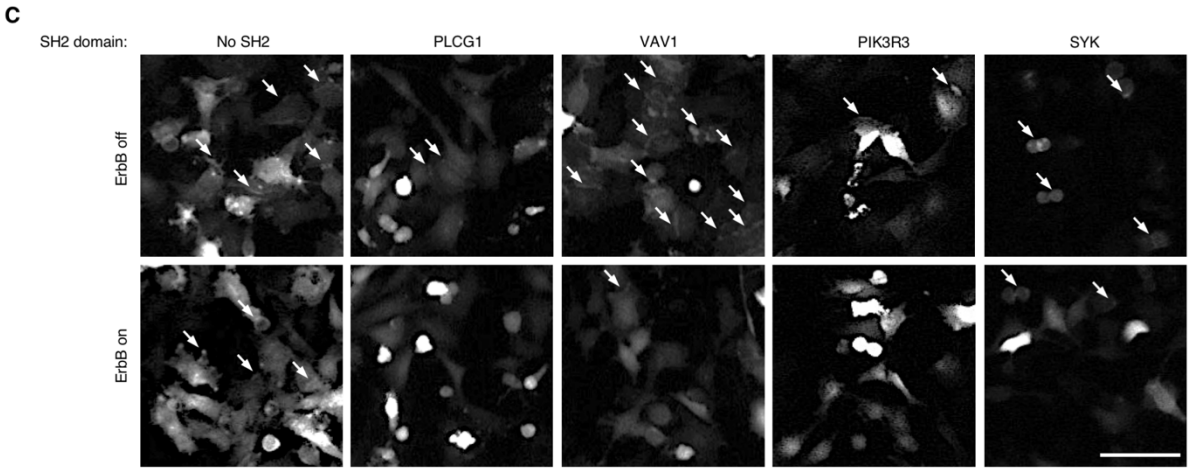

D

Component	$t_{1/2}$ (h)	k_{deg} (h^{-1})	K_{syn} (nM/h)
OFP-DEMEEC-SH2 -CAAX	2.7	0.256	73
cleaved SH2-CAAX	5.0	0.139	NA

Fig. S4. Screening of candidate SH2 domains for substrate co-recruitment. **(a)** LN-229:EGFRvIII cells were transfected with constructs indicated. Cells were left untreated or were treated with lapatinib (lap) to suppress ErbB phosphorylation, then lysed for immunoblot 48 h later. GAPDH served as cell loading control. **(b)** Quantification of released OFP normalized to GAPDH (n = 3, error bars = s.e.m.) for PLCG1, VAV1, SYK, and PI3KR3. Other SH2 domains from (a) were not quantified due to low expression levels. **(c)** ErbB-dependent OFP release without a SH2 domain or with SH2 domains was confirmed qualitatively by direct fluorescence in transfected LN-229:EGFRvIII cells. Arrows, sites of noticeable membrane localization at cell edges. Scale bar, 100 μm. **(d)** Degradation and synthesis rates of SH2-containing substrate fusion proteins. Synthesis rate of OFP-DEMEEC-SH2-CAAX was estimated from that of OFP-DEMEEC-CAAX and their relative expression levels. Synthesis rate of cleaved SH2-CAAX is not applicable (NA) as this protein is synthesized as OFP-DEMEEC-SH2-CAAX.

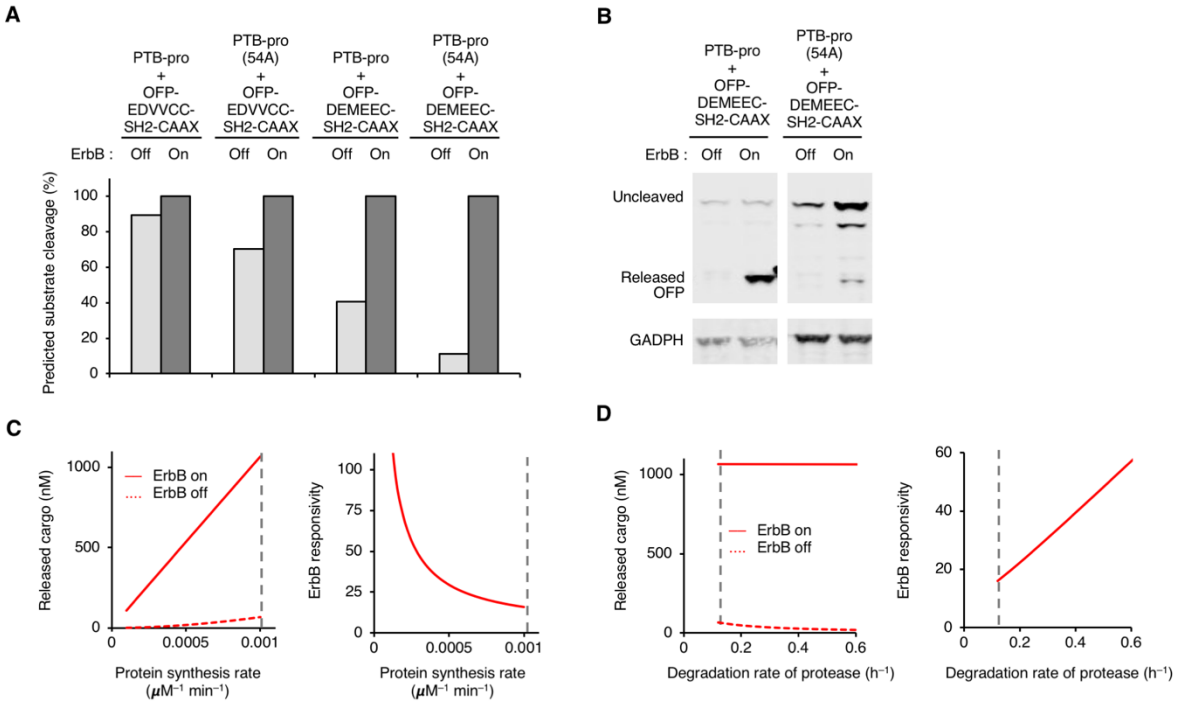

Fig. S5. Modeling assisted RASER improvement. (**A**) Prediction of the percent substrate cleavage of protease and SH2 fused substrate combinations after 24 h of protein expression. (**B**) Constructs indicated were tested in LN-229:EGFRvIII with the same method to (**A**). Blots are from the same membrane. (**C**) Reducing protein synthesis rate for the protease above the value measured in RASER0.2 (vertical dashed line) should increase ErbB dependence of cargo release. (**D**) Faster protease degradation should also increase ErbB dependence of cargo release.

A

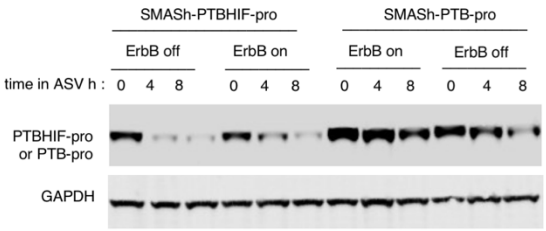

B

	Lapatinib (μM)	$t_{1/2}$ (h)	k_{deg} (h^{-1})
PTBHIF-pro	0.25	2.2	0.318
	0	3.8	0.181
PTB-pro	0.25	5.9	0.117
	0	5.6	0.124

Fig. S6. Measurement of ErbB-dependent stability of PTBHIF-pro by SMASh. (**A**) Stability of PTB-protease fusions with or without ErbB activity was determined by the SMASh system. BT-474 cells were transfected with SMASh-PTBHIF-pro or SMASh-PTB-pro and incubated with or without lapatinib. 24 h later, cells were lysed at 0 h, 4 h, or 8 h after ASV administration. The remaining protein amount were measured by immunoblotting. GAPDH serves as loading control. (**B**) Calculated degradation rates of PTBHIF-pro and PTB-pro.

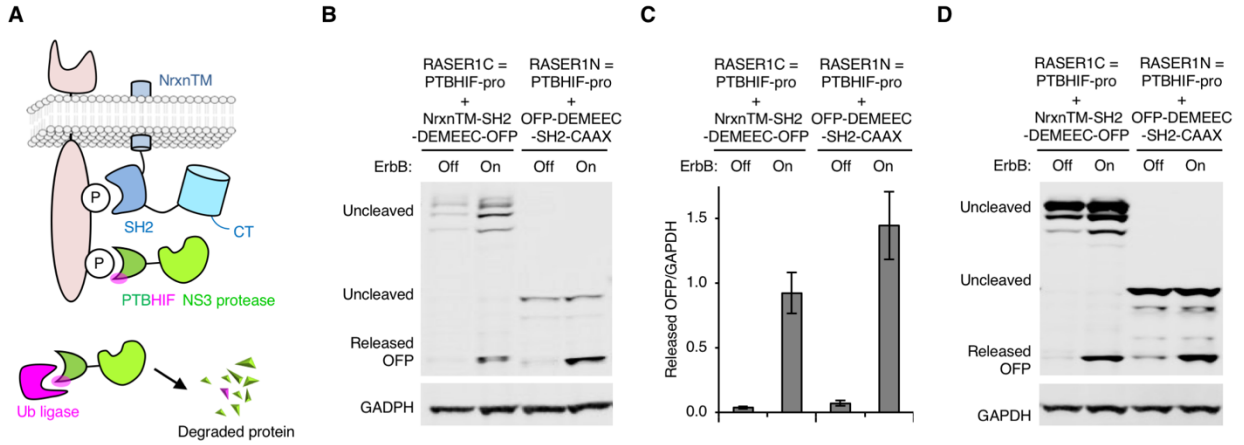

Fig. S7. Generalizing RASER to C-terminally fused cargoes. (**A**) Schematic of the ErbB-RASER1C system, composed of a substrate fusion protein bearing a cargo domain at the C-terminus (NrxnTM-SH2-DEMEEC-cargo) and PTBHIF-pro. (**B**) Both ErbB-RASER1N and ErbB-RASER1C release OFP in an ErbB-dependent manner in BT-474 cells. (**C**) Comparison of ErbB-RASER1N and ErbB-RASER1C outputs in BT-474 cells. (n = 4 and 8 respectively, error bars represent s.e.m.). ErbB responsiveness (output in active relative to inactive states) for RASER1C and RASER1N were 27 ± 7 and 31 ± 6 (mean ± s.e.m.), respectively. (**D**) ErbB responsivity of ErbB-RASER1C and ErbB-RASER1N in MCF-7 cells, which have normal ErbB levels. The cargo is released from ErbB-RASER1N or ErbB-RASER1C only when EGFRvIII is co-expressed.

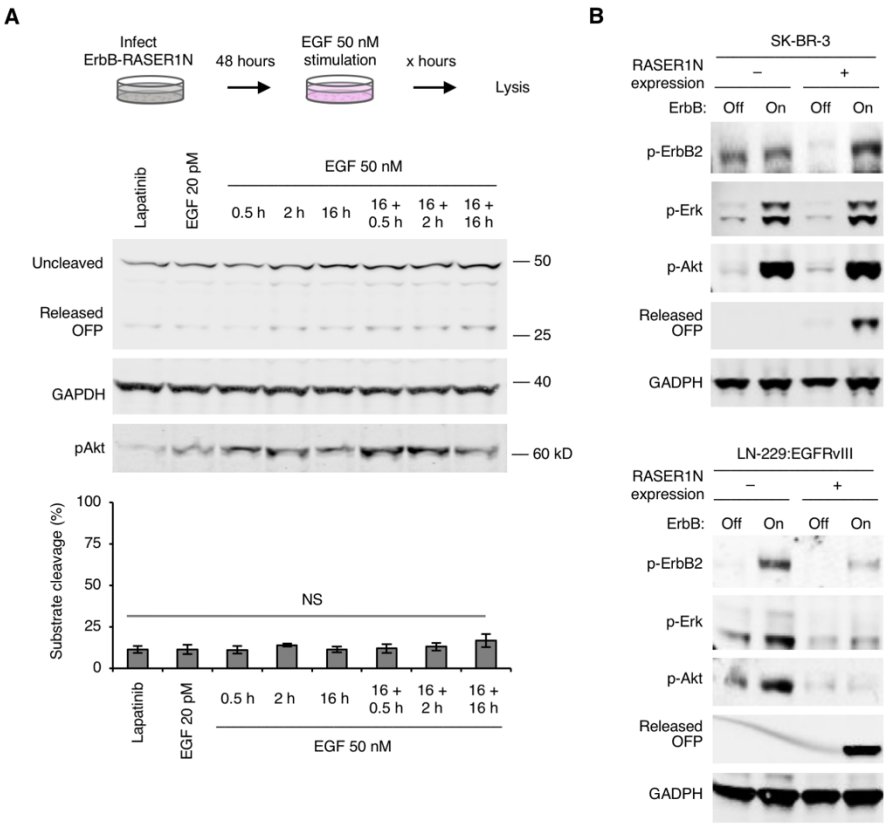

Fig. S8. Additional comparisons of RASER specificity for hyperactive ErbB activity. (**A**) Top, experiment scheme (also for Fig. 4). After 48 h of ErbB-RASER1N expression by lentivirus transduction, ErbB-normal MCF7 cells were stimulated by 50 nM of EGF for various times, followed by cell lysis and immunoblotting. Center, immunoblotting detected uncleaved and released OFP cargo, GAPDH as a loading control, and phosho-Akt (pAkt). EGF stimulation was confirmed by upregulation of pAkt. Size markers are on the right. Bottom, quantitation of substrate cleavage (n = 3, error bars represent s.e.m). Differences between conditions in MCF-7 cells were not significant ($p = 0.73$ in single-factor ANOVA). (**B**) ErbB-RASER1N response and endogenous ErbB downstream activation in SK-BR-3 and LN-229:EGFRvIII cells.

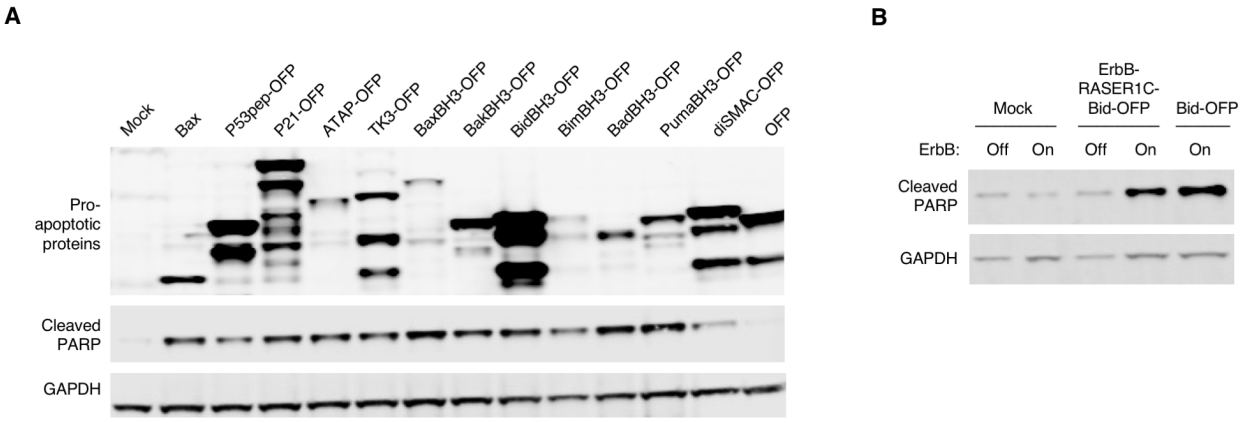

Fig. S9. Programming RASER outputs to rewire constitutive ErbB to apoptosis. (**A**) Screening of apoptosis-inducing cargo. BT-474 cells were transfected with pro-apoptotic proteins and then lysed for immunoblotting 16 h later. Pro-apoptotic protein levels were assessed by blotting for a fused V5 epitope, and induction of apoptosis was assessed by blotting for cleaved PARP. GAPDH served as a loading control. (**B**) PARP cleavage in BT-474 cells transfected with ErbB-RASER1C-Bid-OFP is dependent on ErbB activity, as it is blocked by lapatinib.

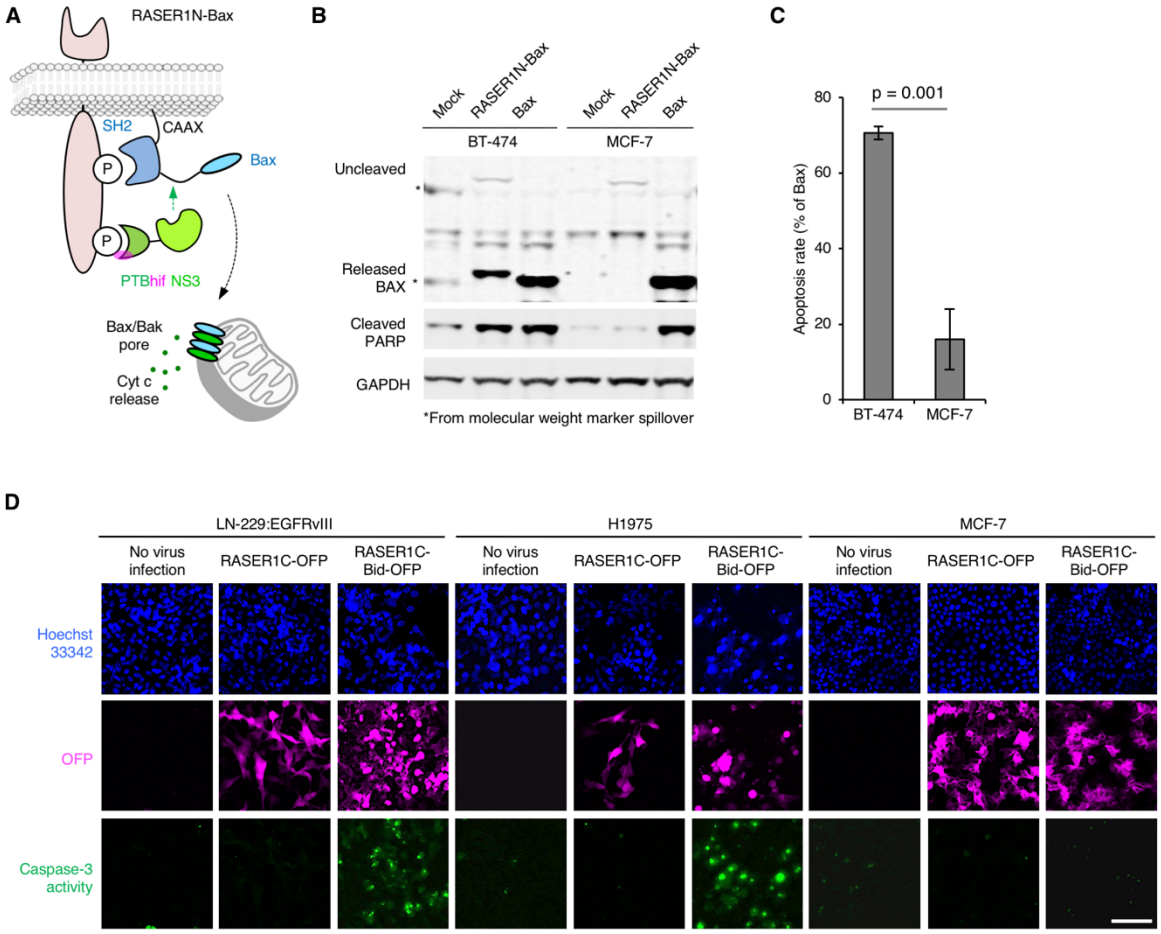

Fig. S10. RASER selectively releases effector cargos to induce apoptosis only in ErbB-hyperactive cancer cells. (**A**) Schematic description of the ErbB-RASER1N-Bax system. Bax monomer will be released in the presence of the tumorigenic ErbB signaling. (**B**) BT-474 cells and MCF-7 cells were transfected with the ErbB-RASER1N-Bax constructs. After 16 h of protein expression, cells were lysed for immunoblotting to detect BAX, cleaved PARP and GAPDH. (**C**) Quantitation of cleaved PARP levels in immunoblots of RASER-transfected cells compared to mock-transfected cells (n = 3, error bars represent s.e.m.). (**D**) Complete set of controls for the experiment of Fig. 5g. Scale bar, 100 μm.

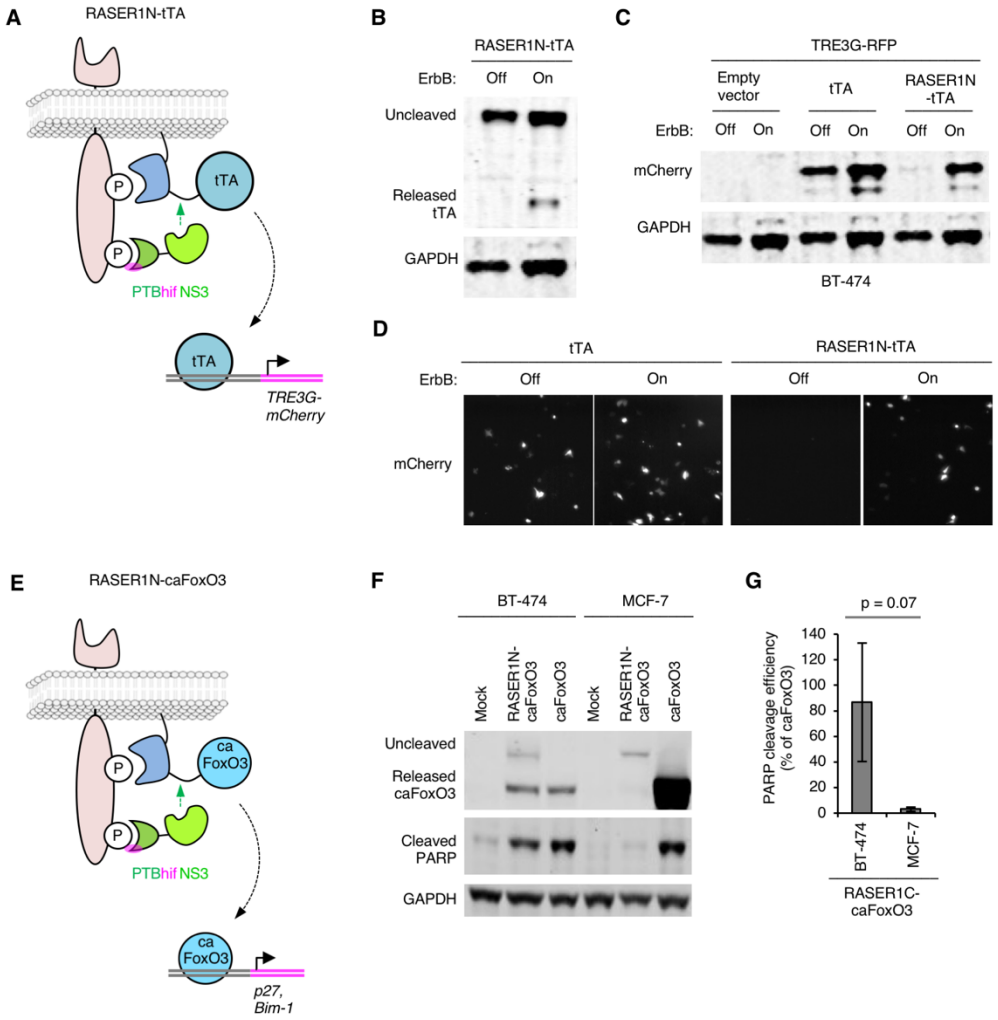

Fig. S11. RASER induced transcription activation. (**A**) A cartoon describes an artificial transcription factor, tTA is released from the RASER system to induce marker gene activation. (**B**) Immunoblot showing the ErbB activity-dependent release of transcription factor, tTA. (**C**) mCherry expression induced by constitutively active tTA or RASER1N-tTA were detected with immunoblotting. (**D**) Fluorescence imaging shows that ErbB-RASER1N-tTA induces mCherry, expression when ErbB2 is hyperactive. (**E**) Schematic description of an ErbB-RASER1N-caFoxO3 system. Constitutively active FoxO3 (caFoxO3) will be released in the presence of hyperactive ErbB to activate pro-apoptotic targets. (**F**) RASER1N-caFoxO3 induces PARP cleavage, a marker of apoptosis, in ErbB-hyperactive BT-474 cells but not in ErbB-normal MCF-7 cells. caFoxO3, cleaved PARP, and GAPDH were assessed by immunoblotting 16 h after transfection. (**G**) Quantitation of immunoblots shows a trend toward more cleavage of PARP in transfected BT-474 cells compared to MCF-7 cells. Significance was assessed by one-tailed unpaired t test. Error bars represent s.e.m. of three biological replicates.

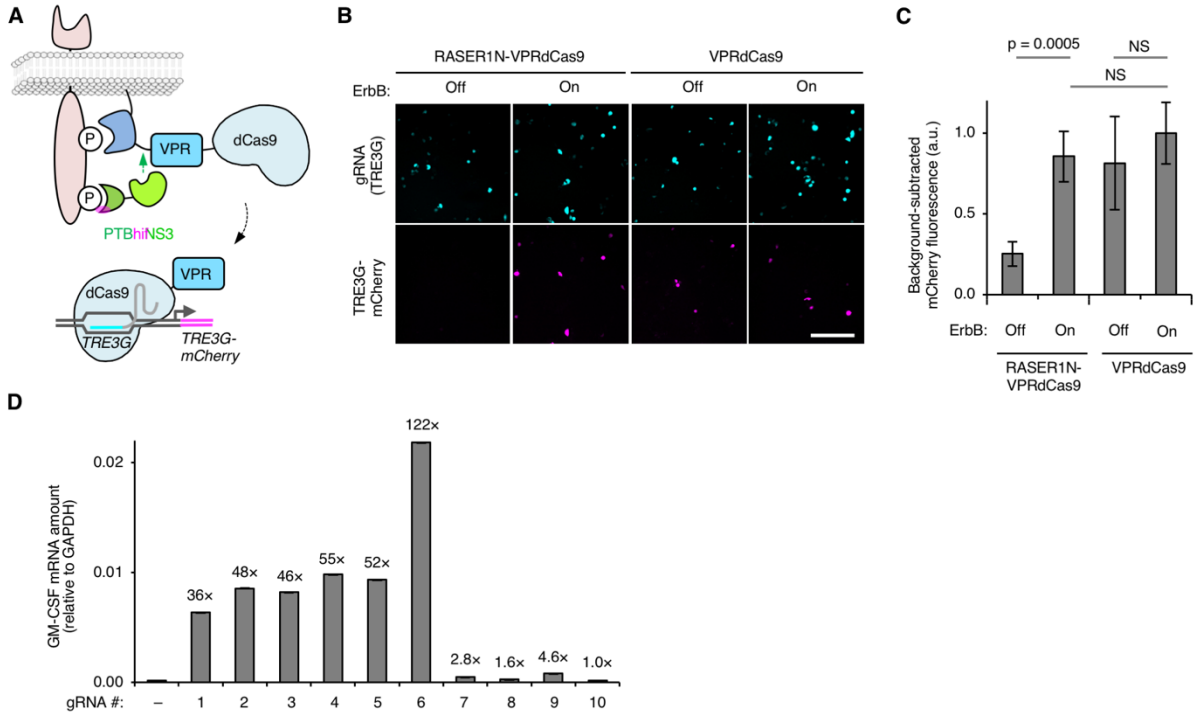

Fig. S12. Programming RASER to rewire constitutive ErbB signaling to transcription. (**A**) Schematic description of an ErbB-RASER1N-VPRdCas9 system, similar to the use of RASERC1 in Fig. 5. (**B**) Fluorescence imaging shows that ErbB-RASER1N-VPRdCas9 induces transcriptional activation of the TRE3G-mCherry reporter gene ErbB2 activation-dependently in BT-474 cells, similar to ErbB-RASERC1-dCas9VP64 in Fig. 6. Scale bar, 500 μm. (**C**) Quantification of (**B**). AU, arbitrary units. NS, not significant. Differences between conditions were assessed by the Kruskal-Wallis test followed by two-tailed Dunn's posthoc tests. $p = 8.8 \times 10^{-5}$ for overall null hypothesis of no difference between groups (n = 40 randomly selected transfected cells, error bars represent s.e.m.). (**D**) Screening of gRNAs to activate GM-CSF transcription. MCF-7 cells were transfected with dCas9VP64, a gRNA containing MS2-binding sequences, and MS2-p65-HSF1. After 24 h, GM-CSF mRNA levels were analyzed by quantitative RT-PCR. Numbers above the bars represent mean fold induction over no gRNA, and error bars represent standard deviation of three technical replicates.

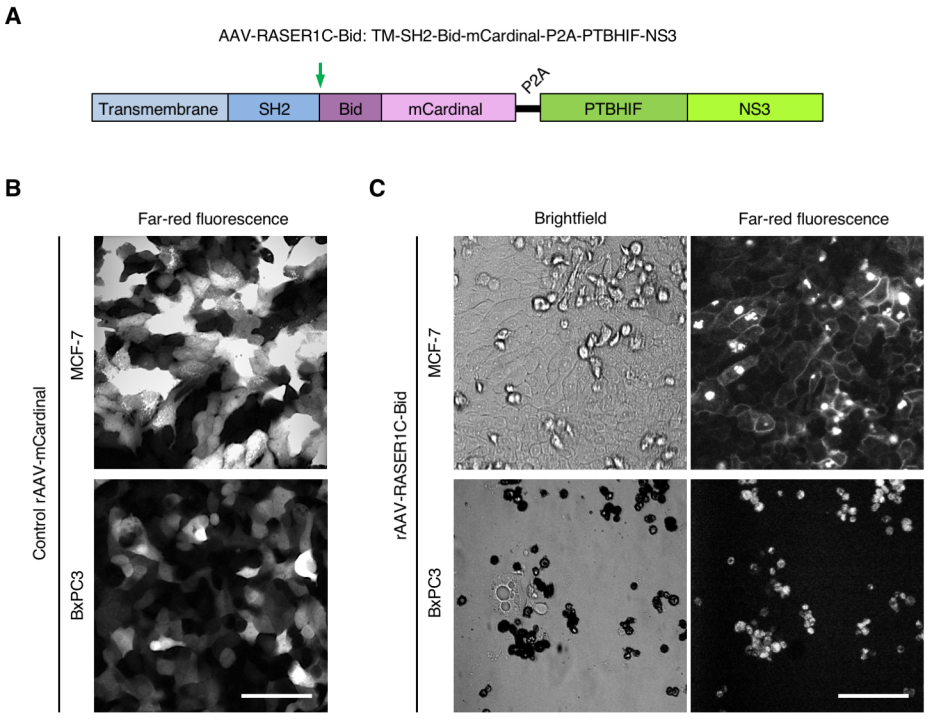

Fig. S13. rAAV-RASER1C-Bid releases the cargo Bid-mCardinal in an ErbB-dependent manner. (**A**) rAAV-RASER1C-Bid expresses a single transcription unit encoding the two RASER components, with the far-red fluorescent protein mCardinal fused to the Bid BH3 domain as the cargo. Green arrow, protease cleavage site to release cargo. (**B**) Control rAAV (rAAV-mCardinal) infection in BxPC3 and MCF-7 cells verifies that both cell lines are well transduced by rAAV without toxicity from the vector alone. (**C**) In ErbB– MCF-7 cells transduced with rAAV-RASER1C-Bid, the Bid-mCardinal cargo is primarily membrane-bound, indicating little RASER activation. By contrast, in ErbB+ BxPC3 cells, Bid-mCardinal is primarily cytosolic, indicating RASER activation. Cells also appear apoptotic in the brightfield image. Scale bars, 100 μm.

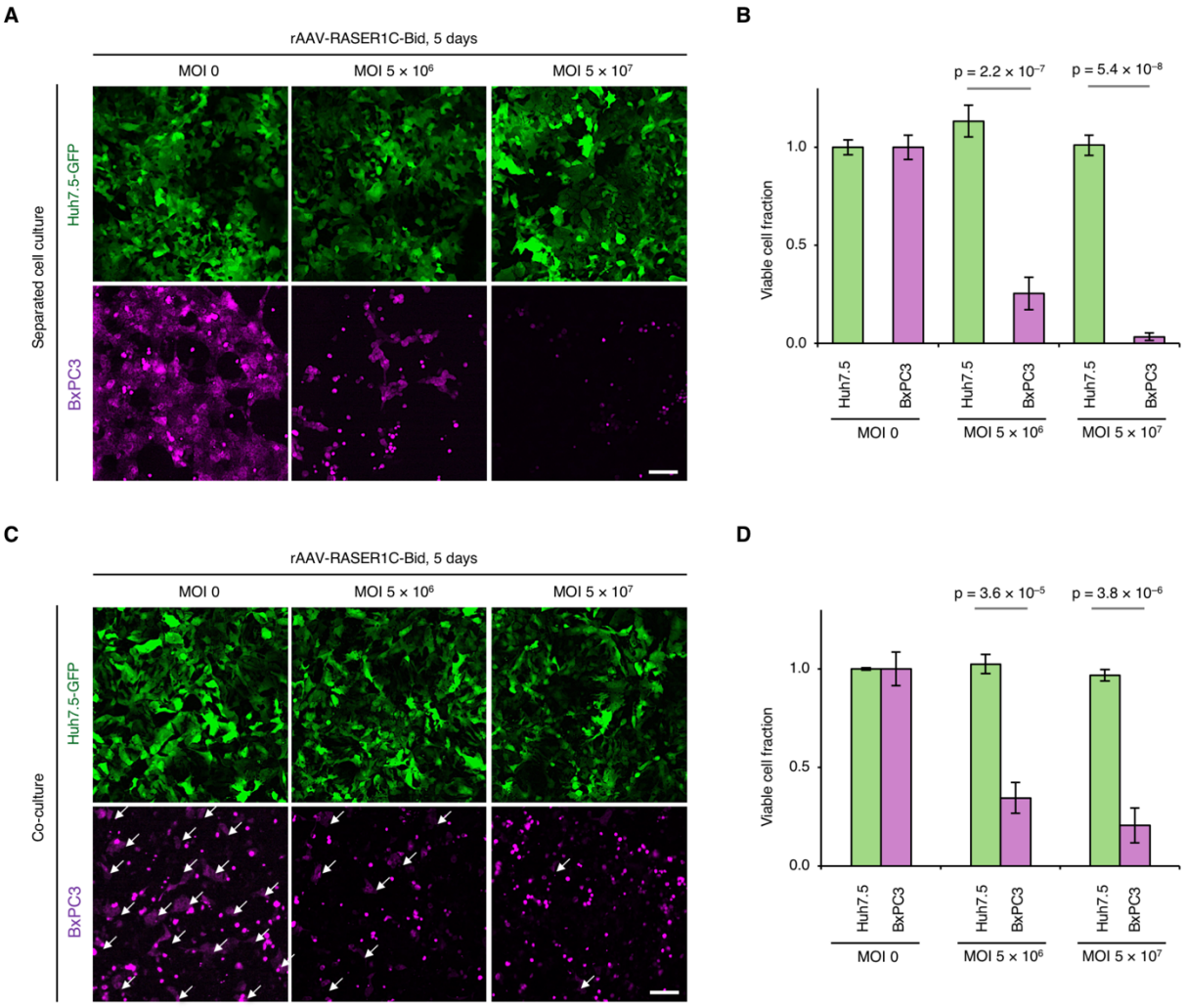

Fig. S14. rAAV-RASER1C-Bid induces death of ErbB-hyperactive cells selectively (**A**) Huh7.5-GFP (green) and BxPC3 (magenta) cells were cultured separately and infected with rAAV-RASER1C-Bid at various MOI. Cells were imaged at 5 days post-infection (DPI). (**B**) Quantitation of imaging shows no difference in the viability of ErbB–Huh7.5-GFP cells, while the number of BxPC3 cells is significantly reduced (n = 4, error bars represent s.e.m.). (**C**) Huh7.5-GFP (green) and BxPC3 (magenta) were co-cultured and infected as described in Fig. 6A. Images were taken on 5 DPI. Colonies of BxPC3 cells were marked with arrows showing the decline in the presence of the RASER virus. (**D**) The RASER virus exclusively targets ErbB-hyperactive BxPC3 cells in the co-culture system (n = 4, error bars represent s.e.m.) Statistical analyses were done by single-factor ANOVA and Holm-Sidak's multiple comparisons test. Scale bar, 100 μm.

References

51. C. A. Schneider, W. S. Rasband, K. W. Eliceiri, NIH Image to ImageJ: 25 years of image analysis. *Nat Methods* **9**, 671-675 (2012). doi: 10.1038/nmeth.2089; pmid: 22930834.
52. E. F. Pettersen *et al.*, UCSF Chimera--a visualization system for exploratory research and analysis. *J. Comput. Chem.* **25**, 1605-1612 (2004). doi: 10.1002/jcc.20084; pmid: 15264254.
53. A. Arkhipov *et al.*, Architecture and membrane interactions of the EGF receptor. *Cell* **152**, 557-569 (2013).
54. M. Y. Hsieh, S. Yang, M. A. Raymond-Stinz, J. S. Edwards, B. S. Wilson, Spatio-temporal modeling of signaling protein recruitment to EGFR. *BMC Syst Biol* **4**, 57 (2010). doi: 10.1016/j.cell.2012.12.030; pmid: 23374350.
55. J. H. Kim *et al.*, High cleavage efficiency of a 2A peptide derived from porcine teschovirus-1 in human cell lines, zebrafish and mice. *PLoS One* **6**, e18556 (2011). doi:10.1371/journal.pone.0018556; pmid: 21602908.
56. P. J. Brennan *et al.*, HER2/neu: mechanisms of dimerization/oligomerization. *Oncogene* **19**, 6093-6101 (2000). doi: 10.1038/sj.onc.1203967; pmid: 11156522.
57. D. Oh *et al.*, Fast rebinding increases dwell time of Src homology 2 (SH2)-containing proteins near the plasma membrane. *Proc. Natl. Acad. Sci. U. S. A.* **109**, 14024-14029 (2012). doi: 10.1073/pnas.1203397109; pmid: 22886086.
58. J. G. Doench *et al.*, Optimized sgRNA design to maximize activity and minimize off-target effects of CRISPR-Cas9. *Nat Biotechnol* **34**, 184-191 (2016). doi: 10.1038/nbt.3437; pmid: 26780180.
59. M. A. Horlbeck *et al.*, Compact and highly active next-generation libraries for CRISPR-mediated gene repression and activation. *Elife* **5**, e19760 (2016). doi: 10.7554/eLife.19760; pmid: 27661255.
60. D. Fattori *et al.*, Probing the active site of the hepatitis C virus serine protease by fluorescence resonance energy transfer. *J. Biol. Chem.* **275**, 15106-15113 (2000). doi: 10.1074/jbc.275.20.15106; pmid: 10809747.
61. A. A. Laminet, G. Apell, L. Conroy, W. M. Kavanaugh, Affinity, specificity, and kinetics of the interaction of the SHC phosphotyrosine binding domain with asparagine-X-X-phosphotyrosine motifs of growth factor receptors. *J. Biol. Chem.* **271**, 264-269 (1996). doi: 10.1074/jbc.271.1.264; pmid: 8550571.